Chemical status of zinc in plant phytoliths: Impact of burning and (paleo)environmental implications

Géraldine Sarret, Eva Schreck, Nathaniel Findling, Damien Daval, Jérôme Viers, Gauthier Delplace, Oleg Pokrovsky

Author version of
Sarret G, Schreck E, Findling N, Daval D, Viers J, Delplace G, et al. Chemical status of zinc in plant phytoliths: Impact of burning and (paleo)environmental implications.
Science of The Total Environment 2022; 852: 158460.
http://dx.doi.org/10.1016/j.scitotenv.2022.158460

Chemical status of zinc in plant phytoliths: impact of burning and (paleo)environmental implications

Géraldine Sarret[1,*], Eva Schreck[2], Nathaniel Findling[1], Damien Daval[1], Jérôme Viers[2], Gauthier Delplace[2], Oleg S. Pokrovsky[2,3]

[1] Univ. Grenoble Alpes, Univ. Savoie Mont Blanc, CNRS, IRD, Univ. G. Eiffel, ISTerre, 38000 Grenoble, France

[2] Géosciences Environnement Toulouse (GET), Université de Toulouse, CNRS, IRD 14 Avenue Edouard Belin, 31400 Toulouse, France

[3] BIO-GEO-CLIM Laboratory, Tomsk State University, Tomsk 634050, Russia

[*] Corresponding author: geraldine.sarret@univ-grenoble-alpes.fr

Highlights

- Dry ashing used for phytolith extraction may favor metal sequestration.
- ICP-MS, XRD, SEM-EDX and EXAFS were used to study chemical and structural changes.
- Dry ashing facilitates Zn incorporation into opal-CT in tetrahedral coordination
- Zn sequestration by phytoliths does not occur *in planta*, but may occur during fire events.
- These results have implications for the reconstruction of paleo fires, and for metal biogeochemical cycles

Abstract

Phytoliths are microscopic structures made of amorphous opal (opal-A), an amorphous hydrated silica, dispersed within plant tissues and persisting after the decay of the plant. Silicon is known to alleviate metal toxicity in plants, but the role of phytoliths in metal sequestration and detoxification is unclear. Dry ashing, the most common protocol for phytolith extraction, was previously shown to lead to sequestration of metals by the phytoliths; however, the mechanisms of this process remained elusive. The purpose of this study was to evaluate whether the association between metals and phytoliths results from dry ashing or pre-exists in plant tissues. Thus, we compared phytoliths extracted by dry ashing at 700°C and plant leaves before and after dry ashing. A combination of ICP-MS, XRD, SEM-EDX and Zn-K-edge EXAFS spectroscopy was used to assess elemental concentrations, morphology and crystallography of silica, and chemical status of Zn. Results demonstrated a phase transition from amorphous opal (opal-A) to opal-CT and α-cristobalite, and the sequestration of metal in phytoliths during dry ashing. For Zn, Mn and Pb, a linear relationship was found between the concentration in phytoliths and in leaves. In the phytoliths, Zn was sequestered in silica in tetrahedral configuration. We hypothesize that this association results form a solid-state reaction during ashing, involving a redistribution of Zn from the organic material to the silica, possibly promoted by the release of structural water from amorphous opal throughout the heating procedure. This study improves our understanding of the impact of high temperature treatments on plant biomass and phytoliths. It suggests that Zn toxicity alleviation in plants by silicon does not rely on its sequestration by phytoliths. In natural settings, wild fire events and biomass burning may lead to metal sequestration in low-soluble form, which should be considered in modeling of biogeochemical cycles and in paleoenvironmental studies.

Graphical abstract

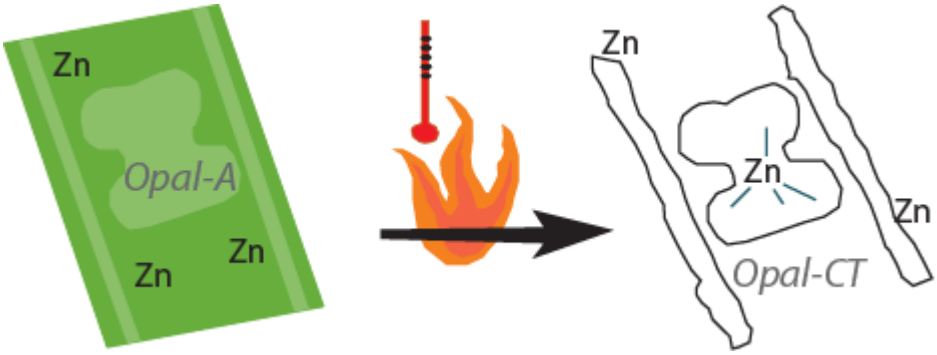

Keywords: phytoliths, Zn, dry ashing, speciation, silica, biogeochemical cycles

Introduction

Silicon (Si) is the second most abundant element in the terrestrial crust, after oxygen. Plants contribute to the biogeochemical cycle of Si through weathering in the rhizosphere, uptake of silicic acid, accumulation and biomineralization within plant tissues (Tran et al., 2019). Phytoliths are microscopic biominerals made of opal-A, a hydrated and amorphous form of silica, $SiO_2 \cdot nH_2O$ (Meunier and Colin, 2001). They are found in some plant tissues (e.g. terrestrial and aquatic plants), particularly in monocotyledons, and they persist after plant decay. Their morphologies are genus and family-specific, so they can be used as proxies of past vegetation in archeology and paleoenvironmental reconstructions (Meunier and Colin, 2001; Piperno, 2006; Sharma et al., 2019). Although silicon is not an essential element for plants, it has a structural role in plant tissues since phytoliths act as a skeleton in non-lignified plant tissues and in some specialized cells like trichomes. In addition, silicon is beneficial for plant fitness, and was shown to alleviate metal toxicity (Adrees et al., 2015). Recent studies have shown the presence of metals and metalloids in phytoliths in plants growing in contaminated environments (Buján, 2013; Lisztes-Szabó et al., 2019; Delplace et al., 2020; Nguyen et al., 2021; Nguyen et al., 2019; Tran et al., 2019). It was suggested that phytoliths are involved in a detoxification mechanism (Buján, 2013; Delplace et al., 2020; Rizwan et al., 2016), and that phytoliths could play an important role in metal (Nguyen et al., 2021; Tran et al., 2019) and carbon (Song et al., 2016) biogeochemical cycle in soils. In a recent review, Hodson and Evans (2020) also showed that co-deposition of Al and Si in phytoliths is a fairly common phenomenon in the plant kingdom, especially in acidic soils, and this may be important in detoxification of Al. Finally, the metal enrichment in phytoliths could be used as geochemical indicator (Buján, 2013) or to trace past activities such as mining in archeology and paleoenvironmental reconstructions (Min et al., 2021), and also for taxonomic identification after discriminant analysis (Lisztes-Szabó et al., 2019).

The most commonly used method for phytolith extraction is dry ashing followed by wet oxidation (Parr et al., 2001; Sharma et al., 2019). The heating treatment is known to slightly alter the morphology of

phytoliths (Parr et al., 2001) and transform amorphous hydrated silica into SiO_2 anhydrous crystalline forms, cristobalite and tridymite (Jones and Milne, 1963; Nguyen et al., 2019). During ashing, metals and accessory elements could be trapped in the phytolith fraction, but the mechanism is not well understood (Jones and Milne, 1963; Nguyen et al., 2019). Thus, a question arises: Does the presence of metals found in phytoliths in previous studies, for example in plants growing in contaminated sites, result from a physiological process such as metal detoxification, or is it an artefact of the separation/purification procedure?

Beside dry ashing during sample pretreatment, phytoliths may be exposed to high temperatures during natural wildfires or agricultural practices involving biomass burning. Thus, the question of the effect of burning on phytoliths and their metal content is important from a paleoenvironmental perspective. Changes in porosity and crystal structure of silica upon heating have been suggested (Devos et al., 2021; Pironon et al., 2001). Based on these changes, phytoliths have been proposed as proxies of paleo-fires based on an increase in auto fluorescence of the phytoliths, although the mechanism responsible for the change in optical properties remains unclear (Devos et al., 2021; Pironon et al., 2001).

Therefore, a better understanding of the status of metal(loid)s associated with phytoliths, and of the possible changes occurring during ashing/burning, is required to evaluate their role of these biominerals in metal detoxification and biogeochemical cycling. Such knowledge is also required to better evaluate the consequences of fire events on metal(loid)s fixation, and is a prerequisite before possible use of phytoliths as a proxy of past contaminations.

Towards this goal, we selected various plant species (essentially monocots and one dicot species), from various sites worldwide, and at various levels of contamination. We characterized the dry leaves and phytoliths extracted by dry ashing procedure, using various spectroscopic and microscopic techniques. Total metal(loid) concentrations were determined by Inductively Coupled Plasma - Mass Spectrometry (ICP-MS). Leaves and phytoliths were then examined by Scanning Electron Microscopy coupled with Energy Dispersive X-ray analysis (SEM-EDX), and phytoliths were characterized by X-Ray Diffraction (XRD). The speciation of Zn in dry leaves, calcinated leaves and phytoliths was studied by extended X-Ray Absorption Fine Structure (EXAFS) spectroscopy. We focused on this element because it is a common metal contaminant, and it was found at high concentrations in some of the samples. Zinc is an essential micronutrient but it is phytotoxic at high concentrations. It is known for its affinity with Si-containing phases in soils (Jacquat et al., 2009; Jacquat et al., 2008) and its ability to sorb onto SiO_2 phases (Nelson et al., 2017) and references therein), and it has been found in phytoliths in previous studies (Buján, 2013; Delplace et al., 2020).

2. Materials and Methods

2.1. Nature and origin of plant samples

Phytoliths were extracted from four plant species: two species of reeds (*Arundo donax* and *Phragmites australis,* monocot species), one species of bamboo (*Phyllostachys bambusoides,* monocot species) and one dicot species of field horsetail (*Equisetum arvense*). A total of 9 specimens were selected, originating from four different sites with various levels of metal(loid) contamination (Table 1):

- The mining district of Cartagena-La Unión, located in the southeast corner of Spain, hosted mining activities for 2000 years, from the 3rd century BCE to the 19th century, mainly for the exploitation of Zn, Pb and Fe (Moreno-Grau et al., 2002). This also led to the mobilization of several other metal(oid)s, such as As, Cd, Cu, Co, Cr, Ni, Sb and Sn and the area is still nowadays considered as contaminated in several of these elements (Blondet et al., 2019; Schreck et al., 2020).

- The mining district of Salsigne, located in southern France, which as extensively exploited between the 4th and the 1st century BCE until the beginning of the 21st century. Mines were first set up to produce Fe, Pb and Cu, then for the exploitation of gold during the 19th century, and finally Salsigne became the biggest mine in the world for As production, until its closure in 2004 (Delplace et al., 2022). Recently, evidence of contamination of streams, sediments and soils in several metal(oid)s have been identified (Delplace et al., 2022; Khaska et al., 2018; Khaska et al., 2015).

- The municipality of Huechún - Tiltil, in the Chacabuco province in Chile, immediately north of Santiago, which is considered as an "environmental sacrifice area" by locals, as the district hosts several tailing dams from mining activities and polluting industries. Arsenic has been found, among other metalloid contaminants, in this area (Le Goff et al., 2022).

- Finally, the urban area of Thái Bình city, northern Vietnam, known for its high-rise buildings, transport infrastructures and heavy road traffic, potentially submitted to urban atmospheric pollution.

2.2. Phytoliths extraction and purification

Phytolith extraction from plant leaves was performed by dry ashing and acid leaching. The most common protocol (Parr 2001) uses a temperature of 500°C. However, several studies which showed the presence of metals in the phytoliths used higher temperatures (600°C in Buján, 2013 and Tran et al., 2019, 700°C in Delplace et al., 2020, up to 900 °C in Nguyen et al., 2021, and up to 1000 °C in Nguyen et al., 2019). In the present study, we used the protocol described in (Delplace et al., 2020), with a temperature of 700°C. This high temperature is in the range of soil temperature during natural wildfires when a large amount of fuel is available (700–800 °C in savannah, 850 °C in chaparral forests, Martinez et al., 2022). Briefly, about 10-20 g of plant material was rinsed with Milli-Q ultrapure water; dried in an oven at 50°C and cut into 1-2 cm pieces. Then, the material was heated in a pre-cleaned porcelain crucible at 700°C for 12 hours to remove organic matter by combustion. Ashes were then transferred from crucibles to polypropylene tubes (0.2 g per tube). Then 10 mL of 10% (m/m) HCl (from 99.999% trace metals basis, Sigma Aldrich®) were added to each tube, and tubes were subsequently put in a water bath at 70°C for 20 min. They were then centrifuged at 4500 rpm for 5 min, and the supernatant was discarded. The remaining material was then rinsed with Milli-Q ultrapure water and centrifuged at 4500 rpm for 5 min, and the supernatant was discarded. Next, 10 mL of 15% (m/m) H_2O_2 (from ≥30% Suprapur, Merck KGaA®) was put into each tube and heated in water bath at 70°C for 20 min. After that, tubes were centrifuged at 4500 rpm for 5 min, and the supernatant was discarded. Finally, the remaining material was rinsed with Milli-Q ultrapure water via repeated centrifugation at 4500 rpm during 5 min, and the supernatant was discarded. Tubes with remaining pellet were then put in an oven and dried at 50°C.

The complete removal of organic matter was checked by measuring the organic C content in the phytoliths with a carbon analyzer (Picarro® G2121i) coupled with a combustion module (Costech®). The organic C content was below the detection limit of the analyzer (0.3 wt%).

2.4. Determination of trace element concentrations in phytoliths and leaves

2.4.1. Determination of trace metal(loi)d concentrations

Aerial parts of plants (100 mg) and phytoliths (around 70 mg) were acid mineralized using 0.2 mL of Suprapur quality HF (48%, Sigma Aldrich®), 8 mL of sub-boiled HNO_3 (15 $mol.L^{-1}$), and 1 mL of H_2O_2 (≥30% Suprapur, Merck KGaA®), added together in closed Teflon vials in a class 10,000 clean room at the GET (Géoscience Environnement Toulouse, France). Acid digestion was performed by CEM® Discover and Millestone® Ultrawave microwave digestion equipments. Blank tests indicated that the level of contamination induced by the acid digestion procedure was negligible, < 2% of the sample

element of interest. Samples were evaporated to dryness, and then diluted in 15 mL of 2% HNO_3. They were diluted again by a factor of 2000. Indium was used as an internal standard. Certified reference material (NIST® SRM® 1515, "Apple leaves") was also processed to check the validity of the analytical procedure.

Concentrations of metal(loid)s were measured on a quadrupole ICP-MS (iCAP Q, Thermo Scientific®-Kinetic Energy Discrimination mode using He) at the AETE-ISO platform (OSU OREME/Université de Montpellier, France). Quantification limits were of 2 ppb for Cu and below 0.2 ppb for all other elements (As, Cd, Mn, Pb, Sb, Sn and Zn). Uncertainties for soils analyses ranged from 1 to 10% for As, Cu, Mn, Pb, Sb and Zn, and from 1 to 20% for Cd and Sn. For plants and phytoliths analyses, uncertainties ranged from 0.1 to 5% for all elements. The agreement between the sample analyses and the certified concentrations was within ± 20% for all elements.

An enrichment factor (denoted EF) was calculated for each element as the ratio between the concentration in phytoliths and the concentration in entire leaves for each element considered, as reported in Equation (1):

Eq (1) $$EF_{(Element)} = \frac{[Element]_{phytoliths}}{[Element]_{leaves}}$$

2.4.2. Statistical analyses

A non-parametric (Kruskal-Wallis) test was used with R software for each element in order to check significant differences between element concentrations in the entire aerial part of plant tissues and in the phytoliths.

2.5. SEM-EDX observations

Environmental SEM observations were performed using a Jeol JSM 6360LV (Jeol®) instrument to characterize the phytolith morphology. Before SEM observations, the phytolith samples were dried and carbon-coated. The apparatus was operated in low-vacuum mode (~133 Pa) at 20 kV. In addition, SEM-EDX analyses were performed on purified phytoliths and on dry leaves for the sample PA-AA, with a Vega3 instrument (Tescan®) equipped with an EDX detector RAYSPEC (30 mm^2), operated in high-vacuum mode at 30 kV for the phytoliths and 16 kV for the dry leaves. The phytoliths and dry leaves cut into small pieces (around 1 mm diameter) were fixed on a carbon tape, and coated with 20 nm carbon before analysis. About 15 EDX analyses were performed on 10 purified phytoliths (bilobate and elongated phytoliths), and 10 EDX analyses on 6 bilobate phytoliths present in dry leaves, and 2 EDX analyses on plant tissue.

2.6. X-ray diffraction (XRD)

The crystalline composition was analyzed by XRD measurements. In this purpose, a concentrated ethanol suspension was dried on a silicon single crystal plate, after low manual grinding in mortar to minimize preferred orientation. XRD data were collected in reflective geometry on an Bruker® diffractometer (D8 Advance, ISTERRE, Grenoble, France), Cu Kα1+2 radiation equipped with a silicon drift detector (Hitachi, USA), and a step size of 0.04° were used to measure from 7 ° to 80° 2θ. The major phases were identified by comparison with JCPDS files in EVA software (Bruker Axs). In addition, Rietveld refinement was performed using the Profex software (Döbelin version 5.0.1*) and a previously determined instrument resolution function. However, due to some experimental limitations (small amount of material available leading to sample transparency and variations in irradiated volume), the quality of the diffraction patterns was not optimal. Therefore, results should be considered as semi-quantitative.

2.7. Zn speciation by EXAFS spectroscopy

Zinc K-edge EXAFS measurements were performed on the beamline SAMBA at the SOLEIL synchrotron (Saint Aubin, France). The monochromator was a Si(220) double crystal. The beam size was 0.4 mm (vertical) x 2 mm (horizontal). Spectra were acquired at room temperature, in continuous scan mode. The fluorescence mode was used for the samples and diluted Zn references (3 min per scan, total acquisition time 30 to 150 min depending on the concentration), and transmission mode for some concentrated Zn references. For each plant, the dry leaves, the calcinated leaves and the phytolith fractions were measured. Data normalization and linear combination fits were achieved using Athena Demeter® software (Athena, Demeter, (Ravel and Newville, 2005)). The library of Zn reference compounds has been described previously (Guiné et al., 2006; Sarret et al., 2006). Three samples of Zn sorbed on amorphous SiO_2 (Zn-SiO_2am) were prepared as follows: a suspension of Zn aerosil 200 (Degussa) was pre-equilibrated at the desired pH (6.0 or 7.2) by addition of NaOH 0.5M, resulting in an ionic strength of 0.5 mM. A Zn nitrate solution was added, and the suspension was stirred for 1h, then centrifuged. The pellet was freeze dried. The concentration of sorbed Zn was determined based on ICP-AES analyses of the initial solution and of the supernatant. Zinc phosphate references included Zn phytate and a mineral specimen containing a mixture of hopeite, parahopeite and tarbuttite, Zn complexed to purified tobacco cell wall at 830 mg kg^{-1} Zn, and in freeze dried state, Zn malate precipitate obtained by slow evaporation of a solution containing 10^{-2} M $Zn(NO_3)_2$ and 8 10^{-2} M Na malate at pH 5.5, and Zn malate in solution (Zn 10 µM, malate 100 µM, pH 5.5, 50% glycerol (this later reference was recorded at 10°K, which may lead to a slight underestimation of the Zn-COOH octahedral pool)).
The spectra for the Zn-SiO_2am were treated by shell fitting using ARTEMIS® software (Ravel and Newville, 2005) to better characterize Zn sorption sites. Zn-O and Zn-Si Paths were calculated using FEFF code, based on the structure of willemite, as done on similar compounds by (Nelson et al., 2017).

3. Results

3.1. Element concentrations in plant tissues and phytoliths

Major and trace element concentrations in entire leaves and in phytoliths are reported in Table 2. The plants were ranked by decreasing Zn content in leaves. The phytoliths exhibited high concentrations in Ca and Mg (up to 3.3 wt% for Ca, 1.1 wt % for Mg), and in other metal(loid)s. *Phragmites australis* seem to highly accumulate trace elements in its tissues, as well as *Arundo donax* to a lesser extent. Moreover, the same plant species accumulate differently according to the sampling site (no bioaccumulation assays (compared to soil metal(loid) contents) were performed in the present study). Plants from the mining districts of Cartagena-La Unión in Spain and Salsigne in France logically appear as the most contaminated ones (especially in Zn, As and Pb as reported in Table 2). The highest Zn content (2852 mg kg^{-1}) was found in *Phragmites australis* from the in Cartagena-La Unión (Table 2). The reeds grown in the province of Chacabuco in Chile (AD-HCN and PA-HCN) present high contents in Cu and Mn (Table 2). By contrast, in the urban area of Thái Bình in Vietnam, the sampled bamboo (B-VIE) does not show really high concentrations in metal(loid)s. Figure 1 focuses on Zn, showing higher Zn concentration in phytoliths compared to leaves, regardless of the site and plant species considered. Elemental ratios between metal(loid) concentration in phytoliths and in leaves, defined as Enrichment Factor (EF, see Materials and Methods section), were > 1 except for As (Table 2). Thus, phytoliths were enriched in Ca, Mg, Mn, Zn, Fe, Cu and Pb compared to the leaves, but not in As. The highest EF were found for Zn, Cu and Pb (21, 23 and 42, respectively, Table 2). The major elements (Ca and Mg) showed lower values of EFs, and As showed the lowest EF (0.1 to 1.5). However, a high variability in EFs was found for a given element and for a given plant species (Table 2). Then, we tested the correlation between metal(loid) concentration in the phytoliths and in the leaves. A significant correlation was

found for Mn, Zn and Pb ($R = 0.980, 0.973, 0.993$, $p < 0.05$), whereas no significant correlation was found for the other elements (Figure 2).

3.2. SEM-EDX investigations on the phytoliths

Observations of purified phytoliths on the different species show typical morphologies of elongated and bilobate phytoliths (International Committee for Phytolith, 2019) (Figures 3 and 4). Some elongated phytoliths have clavate margins (undulated features), as shown in Figure 3A, and correspond to the mineral skeleton of the cell wall. Stomatal structures are also visible for the *Equisetum arevense* samples (Figure 4C1-2). EDX analyses showed that the bilobates had Si and O as major elements, and contained minor amounts of Mg, K and Ca (Figure 3C). In addition, Mn, Cu and Zn were detected in roughly half of the bilobates (8 phytoliths analyzed in total, Figure 3D). The elongated phytoliths had similar elemental composition (Figure SI-1).

For the leaves of *Phragmites australis* from Cartagena-La Unión also investigated by SEM-EDX, bilobate phytoliths embedded in the leaf tissue were observed (Figure 3B). The EDX analyses of these phytoliths showed Si and O as major elements, and minor amounts of S, Cl and K, depending on the samples. No contribution of Ca, Mn, Zn or Cu was detected (Figure 3C and E). Some phytoliths were broken, and it was possible to probe the internal composition by EDX. Again, for these internal parts, no contribution of Ca, Mn, Zn or Cu was detected by EDX (not shown).

3.3. X-Ray Diffraction analyses

Five phytolith samples were characterized by XRD. For the other ones, there was not enough material available. For four samples, the major phase was Opal-CT, and minor amounts of α cristobalite, also called low cristobalite, the low temperature polymorph, quartz, and other accessory minerals were identified (Table 3, Figure 5, Figure SI-2). For the fifth sample (AD-PLG), a broad diffusion band was tentatively attributed to amorphous silica, with probably a large uncertainty on the proportion, and this sample also contained minor amounts of α cristobalite, quartz and other possible minor phases.

3.4. Speciation of Zn in the phytoliths, calcinated leaves and dry leaves

For the same five samples, the speciation of Zn in the phytoliths, calcinated leaves and dry leaves, was determined by Zn K-edge EXAFS spectroscopy (Figure 6). The spectra for the phytoliths were well reproduced by the reference Zn compound sorbed on amorphous SiO_2 (Zn-SiO_2am) at pH 7.2, containing 2433 mg kg^{-1} Zn (Zn-SiO_2am_1_72) (Figure 6, Table 4). In Zn-SiO_2am_1_72, Zn is in tetrahedral coordination (Zn-O distance = 1.94 A), with a weak second shell of Si atoms at 3.52 A, suggesting a disordered environment (Table SI-1, Figure SI-3). In the two others Zn-SiO_2am compounds (i.e., Zn-SiO_2am_01_72 and Zn-SiO_2am_01_60), Zn-O distance is higher (2.00 and 2.02 A), suggesting a mixture of tetrahedral and octahedral coordination (Table SI-1, Figure SI-3). The spectra for the calcinated leaves were very similar to the phytoliths and also matched the Zn-SiO_2am_1_72 reference. For one sample (B-LAS), equivalent fits were obtained with either a mixture of Zn-SiO_2am and Zn phosphate, and with Zn-SiO_2am only. Thus, one can conclude that in the phytoliths and in the calcinated leaves, Zn is essentially tetrahedrally coordinated to silica, in a disordered environment. The dry leaves before ashing had a different spectral signature. Various fits of equivalent quality were obtained, with or without Zn-SiO_2am. Thus, the presence of Zn-SiO_2am in dry leaves cannot be resolved by XAS analysis.

4. Discussion

Phytoliths are known to be composed of SiO_2. However, purified phytoliths contained various major and trace elements including, by decreasing order of importance: Ca, Mg, Fe, Mn, Zn, Cu, Pb and As. They were enriched in these elements compared to the leaves (EF > 1), except in As. The correlation between the concentration of Mn, Zn and Pb in phytoliths and leaves suggests that the amount of metal sequestered in the phytoliths depends on the total amount present in the leaves. This finding does not necessarily imply a physiological control by the plant, as detailed below.

The fact that some divalent metals (Ca, Mg, Mn, Zn) were detected by SEM-EDX in the purified phytoliths, but not in the phytoliths before extraction suggests that these metals were assimilated during the purification procedure. This procedure includes a dry ashing step (700°C during 12h in this study). This burning step induced the transformation from amorphous hydrated silica (opal-A) into opal-CT and a minor fraction of α cristobalite. Opal-CT is composed of disordered material similar to opal-A, and of a small fraction of microcrystalline tridymite, less frequently cristobalite (Wilson, 2014). α cristobalite is a metastable polymorph of SiO_2, previously reported to form either through the cooling of β cristobalite (e.g., (Breneman and Halloran, 2015)) or, more occasionally, directly by epitaxial growth on other mineral substrates (Dera et al., 2011). These structural changes imply a partial removal of structural water present in opal-A (Pironon et al., 2001), which in turn may promote the formation of crystalline phases. In the case of oat phytoliths, Jones and Milne (1963) observed the crystallization of a small proportion of cristobalite after heating at 450°C. Nguyen et al (2019) observed increasing amounts of cristobalite and tridymite in rice phytoliths heated from 700 to 1100°C. In these two papers, the precise form of cristobalite (α or β) was not specified. Contrary to the transition from opal-A to opal-CT and α cristobalite, the solid-state phase transition from these silicate polymorphs to quartz in the present experimental conditions is very unlikely. Thus, quartz could be initially present on leaf surfaces or embedded into biomass as sand particles, which were not removed by washing. Worthy of note, quartz was also identified in purified phytoliths by Jones and Milne (1963) and Nguyen et al. (2019).

The EXAFS analysis of the purified phytoliths showed that they matched the spectrum for Zn sorbed onto amorphous silica (Zn-SiO_2am) prepared in aqueous solution at ambient temperature and pH 7.2. In this compound, Zn is in tetrahedral coordination, with a Si second shell of low amplitude suggesting a disordered environment. This local structure is consistent with a previous study on Zn-SiO_2am prepared in similar conditions (Nelson et al., 2017). Based on the XRD results, the purified phytoliths do not contain amorphous silica (i.e., opal-A) but essentially opal-CT, and a minor proportion of cristobalite. Thus, one can conclude that in the purified phytoliths, Zn is trapped into opal-CT and cristobalite in tetrahedral coordination, in a similar configuration as in a Zn-SiO_2am formed at ambient temperature. Since phytoliths were washed with HCl 10% after ashing, the binding of Zn to opal-CT and cristobalite must be very strong, beyond a simple reversible adsorption mechanism (see below). Thus, Zn is more likely incorporated into opal-CT.

The fact that Zn speciation was similar in purified phytoliths and in calcinated leaves, whereas the association between Zn and silica in dry leaves was uncertain, reinforces the hypothesis that Zn was incorporated in opal-CT during ashing. A recent study showed the synthesis of nanoscale zinc silicate (Zn_2SiO_4), a high temperature mineral with olivine structure, from a mixture of wheat straw (containing phytoliths) and ZnO, in solid state, at temperatures above 1400 °C in an argon atmosphere (Qadri et al., 2017). In the present study, the ashing occurred at lower temperature (700°C) and with no Zn addition. Pironon et al. (2001) showed that the mineralogical transformations occurring during ashing were associated with an increase in the mesoporosity of phytoliths. This phenomenon may favor the sequestration of Zn and other metals in the phytoliths. In addition, the presence of accessory elements during the transformation of silica could favor structural disorder (Jones and Milne, 1963). We propose that Zn originally associated with organic compounds and released during the ashing is then sorbed on the ashes, which are mainly composed of the phytoliths. Zinc sorption to the silica surface in tetrahedral coordination may occur simultaneously to the phase transition from amorphous hydrated silica (opal-A) to opal-CT and, to a minor extent to cristobalite, representing the first elementary step

towards its ultimate irreversible incorporation into the newly formed silica polymorphs. Further studies using the same approach on phytoliths exposed to a range of temperatures could help to further document the transformations.

Nguyen et al. (2021) performed leaching tests on rice straw after dry ashing. They observed a concomitant release of Si and As, and suggested that As could be associated with the phytolith structure, but they did not provide direct evidence for this hypothesis. In the present study, As was not retained in the purified phytolith fraction. Ashing is a strongly oxidizing treatment, so As likely occurs as an oxyanion (i.e., negatively charged) in the phytoliths extracted by dry ashing. Thus, the weak affinity of As for silica (negatively charged) observed in the present study is not surprising.

In natural settings, phytoliths may undergo high temperature treatments during fire events and onsite biomass burning, which is still in use in many regions of the world despite worldwide ban (Nguyen et al., 2021). These heating events should be considered in metal biogeochemical cycles since they may increase the pool of strongly sorbed metals. Conversely, the mineralogical changes upon heating likely influence the solubility of the phytoliths, as well as their reactivity. In basic pH conditions (such as those that may result from fly ash dissolution), the dissolution rates of crystalline tectosilicates are usually lower than those of their amorphous counterparts with identical chemical composition (e.g., (Hamilton et al., 2000; Perez et al., 2019)). Thus, in environmental settings where phytoliths have been subjected to high temperatures (e.g., fire events), their dissolution rates may be lower than those estimated on phytoliths devoid of crystalline phase (e.g., (Fraysse et al., 2009)).

From a paleoenvironmental perspective, the presence of metals associated with the phytoliths should not be interpreted necessarily as a past metallic contamination, since metal incorporation may be strongly enhanced by a heating treatment. The description of the changes in structure, composition and sorption properties of the phytoliths during biomass burning may help to improve their use as proxies of paleo-fires.

Conclusions

The present study shows that the dry ashing protocol, which is the most commonly used for phytolith extraction, leads to (1) the transformation from amorphous hydrated silica (opal-A) into opal-CT and α cristobalite and (2) the incorporation of Zn in these phases. The results obtained for Zn in this work question the role of phytoliths in metal sequestration suggested in previous studies on phytoliths extracted by dry ashing. As such, the known alleviation of metal toxicity in plants by silicon likely results from other processes than metal sequestration by the particles. Future studies on the interactions between metals and phytoliths should use other extraction protocols (and test their possible artefacts), or analyze phytoliths *in situ* in leaf tissues. From an environmental and paleoenvironmental perspective, the changes in structure of silica and speciation of Zn (and other metals) upon heating may affect the biogeochemical cycle of elements. Overall, this study improves our understanding of the changes in structure, composition and sorption properties of the phytoliths during fire events, and may help to better use them as paleoenvironmental proxies.

Contributions

GS: Conceptualization, methodology, validation, formal analyses, data curation, writing - original draft, visualization, funding acquisition ES: Conceptualization, resources, methodology, validation, formal analyses, investigation, data curation, writing - reviewing and editing, visualization, funding acquisition; OP: Conceptualization, writing - reviewing and editing, GD: investigation, data curation, writing - reviewing and editing, NF: investigation, resources, writing - reviewing and editing, DD:

Conceptualization, writing - reviewing and editing, JV: Conceptualization, writing - reviewing and editing. All authors contributed to the article and approved the submitted version.

Acknowledgements

The authors would also like the staff of the platform Geochemistry Mineralogy at ISTerre laboratory, and the staff of the AETE-ISO « Analyse des Eléments en Trace dans l'Environnement & ISOtopes » platform in Montpellier, France. We also thank the synchrotron SOLEIL for the provision of beamtime, Gautier Landrot and the beamline staff on Samba for their help with the measurements, Thierry Aigouy for his help with the SEM-EDX observations, and Eloi Lasserre for his support in phytolith extraction in the GET laboratory. This work was carried out as part of the interdisciplinary "CARE" project through the French MITI/CNRS funding program. Additional funding was provided by BQR ISTerre. ISTerre is part of Labex OSUG (ANR10 LABX56). OP thanks the TSU Development Program Priority-2030.

References

Adrees M, Ali S, Rizwan M, Zia-ur-Rehman M, Ibrahim M, Abbas F, et al. Mechanisms of silicon-mediated alleviation of heavy metal toxicity in plants: A review. Ecotoxicology and Environmental Safety 2015; 119: 186-197.

Blondet I, Schreck E, Viers J, Casas S, Jubany I, Bahí N, et al. Atmospheric dust characterisation in the mining district of Cartagena-La Unión, Spain: Air quality and health risks assessment. Science of The Total Environment 2019; 693: 133496.

Breneman RC, Halloran J. Hysteresis upon Repeated Cycling through the Beta-Alpha Cristobalite Transformation. Journal of Ceramic Science and Technology 2015; 6: 55-61.

Buján E. Elemental composition of phytoliths in modern plants (Ericaceae). Quaternary International 2013; 287: 114-120.

Delplace G, Schreck E, Pokrovsky OS, Zouiten C, Blondet I, Darrozes J, et al. Accumulation of heavy metals in phytoliths from reeds growing on mining environments in Southern Europe. Science of The Total Environment 2020; 712: 135595.

Delplace G, Viers J, Schreck E, Oliva P, Behra P. Pedo-geochemical background and sediment contamination of metal(loid)s in the old mining-district of Salsigne (Orbiel valley, France). Chemosphere 2022; 287: 132111.

Dera P, Lazarz JD, Prakapenka VB, Barkley M, Downs RT. New insights into the high-pressure polymorphism of SiO2 cristobalite. Physics and Chemistry of Minerals 2011; 38: 517-529.

Devos Y, Hodson MJ, Vrydaghs L. Auto-Fluorescent Phytoliths: A New Method for Detecting Heating and Fire. Environmental Archaeology 2021; 26: 388-405.

Fraysse F, Pokrovsky OS, Schott J, Meunier J-D. Surface chemistry and reactivity of plant phytoliths in aqueous solutions. Chemical Geology 2009; 258: 197-206.

Guiné V, Spadini L, Sarret G, Muris M, Delolme C, Gaudet JP, et al. Zinc sorption to three gram-negative bacteria: Combined titration, modeling, and EXAFS study. Environ. Sci. Technol. 2006; 40: 1806-1813.

Hamilton JP, Pantano CG, Brantley SL. Dissolution of albite glass and crystal. Geochimica et Cosmochimica Acta 2000; 64: 2603-2615.Hodson MJ and Evans DE. Aluminium/silicon interactions in higher plants-an update. Journal of Experimental Botany 2020; 71: 6719-6729. https://doi.org/10.1093/jxb/eraa024

International Committee for Phytolith T. International Code for Phytolith Nomenclature (ICPN) 2.0. Annals of botany 2019; 124: 189-199.

Jacquat O, Voegelin A, Kretzschmar R. Local coordination of Zn in hydroxy-interlayered minerals and implications for Zn retention in soils. Geochim. Cosmochim. Acta 2009; 73: 348-363.

Jacquat O, Voegelin A, Villard A, Marcus M, Kretzschmar R. Formation of Zn-rich phyllosilicate, Zn-layered double hydroxide and hydrozincite in contaminated calcareous soils. Geochim. Cosmochim. Acta 2008; 72: 5037-5054.

Jones LHP, Milne AA. Studies of silica in the oat plant. Plant and Soil 1963; 18: 207-220.

Khaska M, Le Gal La Salle C, Sassine L, Cary L, Bruguier O, Verdoux P. Arsenic and metallic trace elements cycling in the surface water-groundwater-soil continuum down-gradient from a reclaimed mine area: Isotopic imprints. Journal of Hydrology 2018; 558: 341-355.

Khaska M, Le Gal La Salle C, Verdoux P, Boutin R. Tracking natural and anthropogenic origins of dissolved arsenic during surface and groundwater interaction in a post-closure mining context: Isotopic constraints. Journal of Contaminant Hydrology 2015; 177-178: 122-135.

Le Goff L, Blot F, Peltier A, Laffont L, Becerra S, Henríquez Ruiz C, et al. From uncertainty to environmental impacts: reflection on the threats to water in Chacabuco Province (Chile): a combined approach in social sciences and geochemistry. Sustainability Science 2022.

Lisztes-Szabó Z, Braun M, Csík A *et al.* Phytoliths of six woody species important in the Carpathians: characteristic phytoliths in Norway spruce needles. Veget Hist Archaeobot 2019; 28: 649–662.

Martínez SI, Contreras CP, Acevedo SE, Bonilla CA. Unveiling soil temperature reached during a wildfire event using ex-post chemical and hydraulic soil analysis. Science of The Total Environment 2022; 822: 153654.Meunier J, Colin F. Phytoliths: applications in earth sciences and human history. A. A. Balkema Publishers, 2001.

Min H-G, Kim M-S, Kim J-G. Effect of Soil Characteristics on Arsenic Accumulation in Phytolith of Gramineae (Phragmites japonica) and Fern (Thelypteris palustris) Near the Gilgok Gold Mine. Sustainability 2021; 13.

Moreno-Grau S, Cascales-Pujalte JA, MartÍnez-GarcÍa MJ, Angosto JM, Moreno J, Bayo J, et al. Relationships between Levels of Lead, Cadmium, Zinc, and Copper in Soil and Settleable Particulate Matter in Cartagena (Spain). Water, Air, and Soil Pollution 2002; 137: 365-383.

Nelson J, Wasylenki L, Bargar JR, Brown GE, Maher K. Effects of surface structural disorder and surface coverage on isotopic fractionation during Zn(II) adsorption onto quartz and amorphous silica surfaces. Geochimica et Cosmochimica Acta 2017; 215: 354-376.

Nguyen MN, Dam TTN, Nguyen ATQ, Nguyen AM, Nguyen LN, Duong LT, et al. Arsenic in rice straw phytoliths: Encapsulation and release properties. Applied Geochemistry 2021; 127: 104907.

Nguyen TN, Nguyen MN, McNamara M, Dultz S, Meharg A, Nguyen VT. Encapsulation of lead in rice phytoliths as a possible pollutant source in paddy soils. Environmental and Experimental Botany 2019; 162: 58-66.

Parr JF, Lentfer CJ, Boyd WE. A Comparative Analysis of Wet and Dry Ashing Techniques for the Extraction of Phytoliths from Plant Material. Journal of Archaeological Science 2001; 28: 875-886.

Perez A, Daval D, Fournier M, Vital M, Delaye J-M, Gin S. Comparing the reactivity of glasses with their crystalline equivalents: The case study of plagioclase feldspar. Geochimica et Cosmochimica Acta 2019; 254: 122-141.

Piperno DR. Phytoliths: a comprehensive guide for archaeologists and paleoecologists: AltaMira Press, Lanham, MD, 2006.

Pironon J, Meunier J, Alexandre A, Mathieu R, Mansuy L, Grosjean A, et al. Individual characterizaiton of phytoliths: Experimental approach and consequences on paleoenvironmental understanding. In: Meunier J, Colin F, editors. Phytoliths: applications in earth sciences and human history. A. A. Balkema Publishers, 2001, pp. 329-341.

Qadri SB, Gorzkowski EP, Rath BB, Feng CR, Amarasinghe R, Freitas JA, et al. Nanoscale zinc silicate from phytoliths. Journal of Crystal Growth 2017; 476: 25-30.

Ravel B, Newville M. ATHENA and ARTEMIS: Interactive graphical data analysis using IFEFFIT. J. Synchr. Rad. 2005; 12: 537-541.

Rizwan M, Meunier JD, Davidian JC, Pokrovsky OS, Bovet N, Keller C. Silicon alleviates Cd stress of wheat seedlings (Triticum turgidum L. cv. Claudio) grown in hydroponics. Environmental Science and Pollution Research 2016; 23: 1414-1427.

Sarret G, Harada E, Choi YE, Isaure MP, Geoffroy N, Fakra S, et al. Trichomes of tobacco excrete zinc as zinc-substituted calcium carbonate and other zinc-containing compounds. Plant Physiology 2006; 141: 1021-1034.

Schreck E, Viers J, Blondet I, Auda Y, Macouin M, Zouiten C, et al. Tillandsia usneoides as biomonitors of trace elements contents in the atmosphere of the mining district of Cartagena-La Unión (Spain): New insights for element transfer and pollution source tracing. Chemosphere 2020; 241: 124955.

Sharma R, Kumar V, Kumar R. Distribution of phytoliths in plants: a review. Geology, Ecology, and Landscapes 2019; 3: 123-148.

Song Z, McGrouther K, Wang H. Occurrence, turnover and carbon sequestration potential of phytoliths in terrestrial ecosystems. Earth-Science Reviews 2016; 158: 19-30.

Tran TTT, Nguyen TT, Nguyen VT, Huynh HTH, Nguyen TTH, Nguyen MN. Copper encapsulated in grass-derived phytoliths: Characterization, dissolution properties and the relation of content to soil properties. Journal of Environmental Management 2019; 249: 109423.

Wilson MJ. The structure of opal-CT revisited. Journal of Non-Crystalline Solids 2014; 405: 68-75.

Table 1 : Plant species studied and sampling location

Sample identification	*Species*	*Origin*	*GPS coordinates*
PA-AA	*Phragmites Australis*	Cartagena (Spain)	37.594469, -0.883927
PA-SA	*Phragmites Australis*	Cartagena (Spain)	37.596037, -0.885870
PA-HCH	*Phragmites Australis*	Chacabuco (Chile) – Huechún	-33.086094, -70.798887
AD-PLG	*Arundo Donax*	Cartagena (Spain)	37.579087 - 0.875813
AD-LAS	*Arundo Donax*	Salsigne (France)	43.308846, 2.393615
AD-HCH	*Arundo Donax*	Chacabuco (Chile) – Huechún	-33.086094, -70.798887
PRE-LAS	*Equisetum arvense*	Salsigne (France)	43.308846, 2.393615
B-LAS	*Phyllostachys bambusoides*	Salsigne (France)	43.308846, 2.393615
B-VIE	*Phyllostachys bambusoides*	Thái Bình (Vietnam)	20.471097, 106.364332

Table 2 : Elemental concentrations in phytoliths and plant leaves of the four species of plant, and enrichment factors [a]

			Concentrations (mg kg-1)							
Sample ID	**Type**	**Species**	**Ca**	**Mg**	**Fe**	**Zn**	**As**	**Cu**	**Mn**	**Pb**
PA-AA	Phytoliths	*Phragmites Australis*	8576 ± 429	5694 ± 285	1507 ± 90	2852 ± 86	1.93 ± 0.12	69.7 ± 3.5	1659 ± 50	379.0 ± 11.4
PA-AA-F	Leaves		3064 ± 153	3411 ± 171	444 ± 27	355 ± 11	6.04 ± 0.36	6.9 ± 0.3	412 ± 12	45.5 ± 1.4
			EF = 2.8	***EF = 1.7***	***EF = 3.4***	***EF = 8.0***	***EF = 0.3***	***EF = 10.1***	***EF = 4.0***	***EF = 8.3***
PA-SA	Phytoliths	*Phragmites Australis*	17628 ± 881	10348 ± 517	448 ± 27	577 ± 17	0.08 ± 0.00	51.8 ± 2.6	2619 ± 79	36.5 ± 1.1
PA-SA-F	Leaves		4373 ± 219	4948 ± 247	122 ± 7	41 ± 1	0.71 ± 0.04	3.7 ± 0.2	880 ± 26	6.2 ± 0.2
			EF = 4.0	***EF = 2.1***	***EF = 3.7***	***EF = 14.0***	***EF = 0.1***	***EF = 14.0***	***EF = 3.0***	***EF = 5.9***
AD-LAS	Phytoliths	*Arundo Donax*	21372 ± 1069	6278 ± 314	858 ± 51	546 ± 16	0.54 ± 0.03	115.8 ± 5.8	448 ± 13	21.0 ± 0.6
AD-LAS-F	Leaves		6184 ± 309	840 ± 42	190 ± 11	34 ± 1	1.56 ± 0.09	5.1 ± 0.3	34 ± 1	1.7 ± 0.1
			EF = 3.5	***EF = 7.5***	***EF = 4.5***	***EF = 15.9***	***EF = 0.3***	***EF = 22.9***	***EF = 13.3***	***EF = 12.0***
PRE-LAS	Phytoliths	*Equiseteum arvense*	21568 ± 1078	6447 ± 322	1155 ± 69	443 ± 13	4.88 ± 0.29	22.3 ± 1.1	85 ± 3	14.4 ± 0.4
PRE-LAS-F	Leaves		20263 ± 1013	2793 ± 140	274 ± 16	93 ± 3	4.01 ± 0.24	6.9 ± 0.3	24 ± 1	1.7 ± 0.0
			EF = 1.1	***EF = 2.3***	***EF = 4.2***	***EF = 4.7***	***EF = 1.2***	***EF = 3.3***	***EF = 3.5***	***EF = 8.6***
B-LAS	Phytoliths	*Phyllostachys bambusoides*	33484 ± 1674	11282 ± 564	1841 ± 110	425 ± 13	1.82 ± 0.11	93.0 ± 4.6	186 ± 6	42.5 ± 1.3
B-LAS-F	Leaves		5750 ± 288	1654 ± 83	238 ± 14	20 ± 1	1.97 ± 0.12	7.8 ± 0.4	17 ± 1	1.5 ± 0.0
			EF = 5.8	***EF = 6.8***	***EF = 7.7***	***EF = 21.1***	***EF = 0.9***	***EF = 12.0***	***EF = 10.7***	***EF = 27.5***
AD-HCH	Phytoliths	*Arundo Donax*	25344 ± 1267	9700 ± 485	913 ± 55	96 ± 3	0.11 ± 0.01	67.6 ± 3.4	453 ± 14	3.2 ± 0.1
AD-HCH-F	Leaves		3780 ± 189	1835 ± 92	92 ± 6	35 ± 1	0.08 ± 0.00	10.0 ± 0.5	47 ± 1	0.1 ± 0.0
			EF = 6.7	***EF = 5.3***	***EF = 9.9***	***EF = 2.7***	***EF = 1.5***	***EF = 6.7***	***EF = 9.6***	***EF = 41.8***
B-VIE (T1)	Phytoliths	*Phyllostachys bambusoides*	32346 ± 1617	7217 ± 361	1741 ± 104	145 ± 4	0.55 ± 0.03	48.0 ± 2.4	472 ± 14	41.6 ± 1.2
B-VIE-F (T1)	Leaves		4906 ± 245	1184 ± 59	240 ± 14	14 ± 0	0.43 ± 0.03	3.6 ± 0.2	56 ± 2	1.7 ± 0.1
			EF = 6.6	***EF = 6.1***	***EF = 7.3***	***EF = 10.3***	***EF = 1.3***	***EF = 13.3***	***EF = 8.5***	***EF = 24.5***
PA-HCH	Phytoliths		13636 ± 682	8840 ± 442	694 ± 42	135 ± 4	0.41 ± 0.02	166.5 ± 8.3	905 ± 27	32.6 ± 1.0

PA-HCH-F	Leaves	*Phragmites Australis*	8981	±	449	4995	±	250	216	±	13	19	±	1	0.77	±	0.05	8.3	±	0.4	315	±	9	1.1	±	0.0
			EF	***=***	***1.5***	***EF***	***=***	***1.8***	***EF***	***=***	***3.2***	***EF***	***=***	***7.1***	***EF***	***=***	***0.5***	***EF***	***=***	***20.1***	***EF***	***=***	***2.9***	***EF***	***=***	***30.9***

[a] For each element, the enrichment factor was calculated as $[element]_{phytoliths}$/ $[element]_{leaves}$.

Table 3: Phases identified by XRD (in weight %)

	Opal-CT	α Cristobalite (low)	Quartz	Sylvite	Amorphous phase *	Other possible minor phases
PA-AA	96.0	1.5	1.1	0.4		Mg phosphate, nepheline
PA-SA	97.5	1.4		1.11		
B-LAS	99.0		1.0			
PRE-LAS	98.2		1.8			
AD-PLG		2.3	1.6		87.5	Diopside, Mg sulfate hydroxide, Mg phosphate, Na Ca phosphate

Sylvite: KCl, Nepheline: $(Na,K)AlSiO_4$, Diopside $CaMgSi_2O_6$, Mg sulfate hydroxide : $Mg_3S2O_8(OH)_2/2MgSO_4{\cdot}Mg(OH)_2$, Mg phosphate : $Mg_2P_4O_{12}$, Na,Ca phosphate : $MgCaP_4O_{12}$. *: Si-containing amorphous phase, simulated by a broad band centered on the main reflexion of quartz.

Table 4. Percentage of Zn species in the phytoliths, calcinated leaves (C) and dry leaves (F) determined by linear combination fits.

	Fitting range in k space ($Å^{-1}$)	Zn-SiO_2am tetra [a]	Zn phos-phate [b]	Zn-COOH tetra. [c]	Zn-COOH interm. [d]	Zn-COOH octa. [e]	Sum	R factor[f]
Phytoliths								
PA-AA	2.5-12	109					109	0.057
PA-SA	2.5-12	106					106	0.055
AD-PLG	2.5-12	119					119	0.069
B-LAS	2.5-12	111					111	0.041
PRE-LAS	2.5-12	107					107	0.047
Calcinated leaves								
PA-AA-C	2.5-12.5	100					100	0.036
PA-SA-C	2.5-12.5	118					118	0.19165
AD-PLG-C	2 to 12.9	111					111	0.065
B-LAS C	2.5-12.5	36	65				101	0.048
		103					103	0.053
PRE-LAS-C	2.5-11.5	109					109	0.078
Dry leaves								
PA-AA-F	2.5-11	20			53		73	0.021
			20		52		72	0.024
PA-SA-F	2.5-11.5	40		26		34	100	0.065
		42	16			41	99	0.068
			37	29		33	99	0.072
AD-PLG-F	2.5-11.5	32	18			50	100	0.056
			29		18	39	86	0.058
				28	30	24	82	0.06
B-LAS F	2.5-11.5	34		38	25		97	0.077
		39	8		41		88	0.084
PRE-LAS-F	2.5-11.5	56		30		24	110	0.049
		54	23	31			108	0.052

Reference compounds used for each family: a, Zn-SiO_2am_1_72, b, Zn phytate or hopeite, c, Zn-cell wall, d, Zn malate precipitate, e, Zn malate in solution. F, [a] R factor (residual between fit and measured) = $\sum[k^2 \chi_{exp} - k^2 \chi_{fit}]^2 / \sum[k^2 \chi_{exp}]^2$. For B-LAS-C and for the dried leaves, several fits of equivalent quality (increase of R factor < 15% compared to the best fit) were obtained. The sum of percentages may exceed 100%, due to slight differences in the normalization, and/or slight structural differences of Zn local structure between reference compounds and samples.

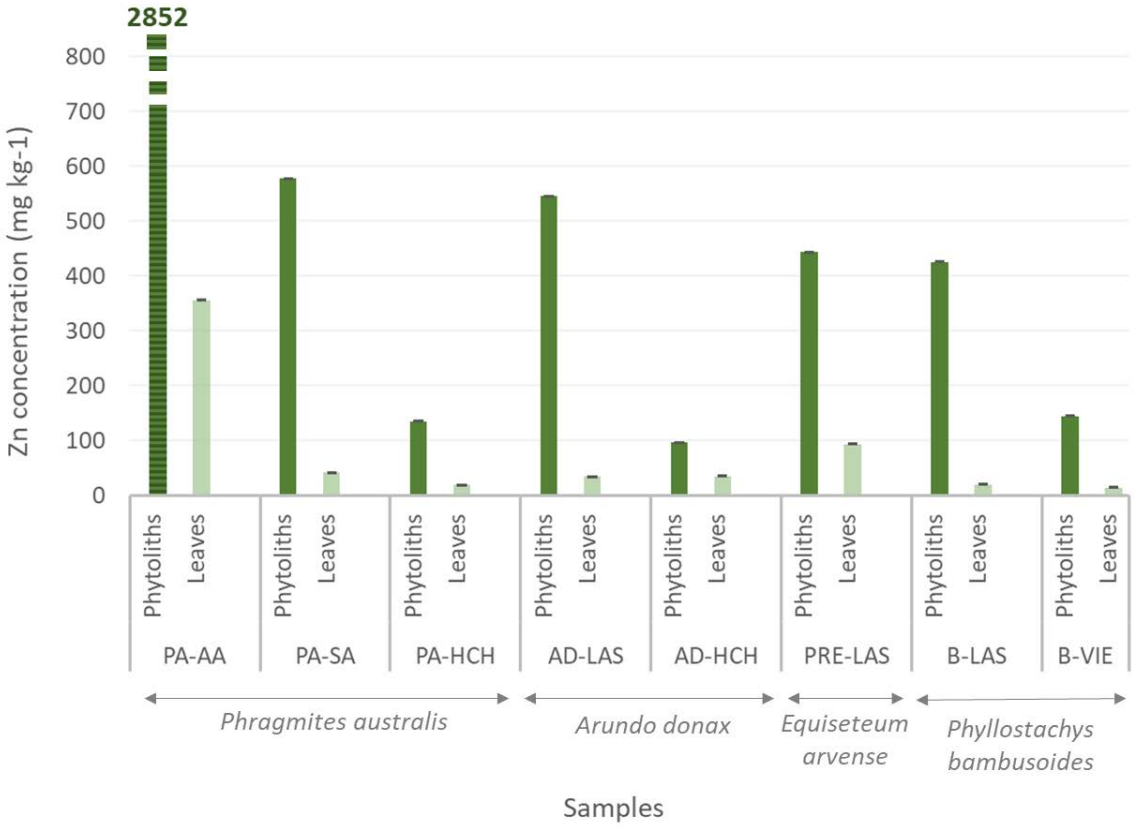

Figure 1. Zn concentration (in mg kg^{-1} of dry weight) in purified phytoliths and in entire leaves for the four plant species.

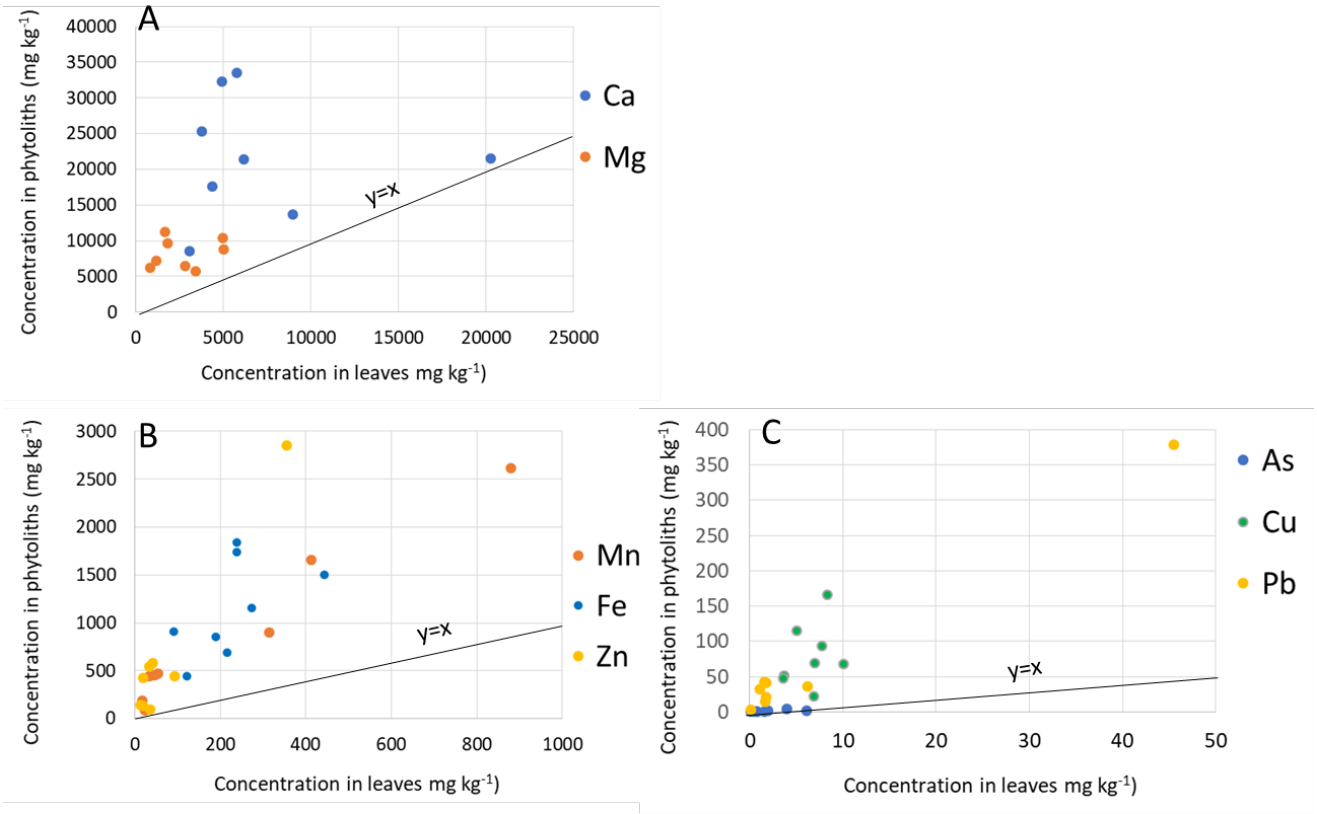

Figure 2. Metal(loid) concentration in phytoliths as a function of their concentration in leaves. The correlation coefficient R calculated for each element was: Ca: -0.012, Mg: 0.206, Mn: 0.980, Fe: 0.564, Zn: 0.973, As: 0.692, Cu: 0.308, Pb: 0.993. The correlation was statistically significant (p-value < 0.05) for Zn, Mn and Pb.

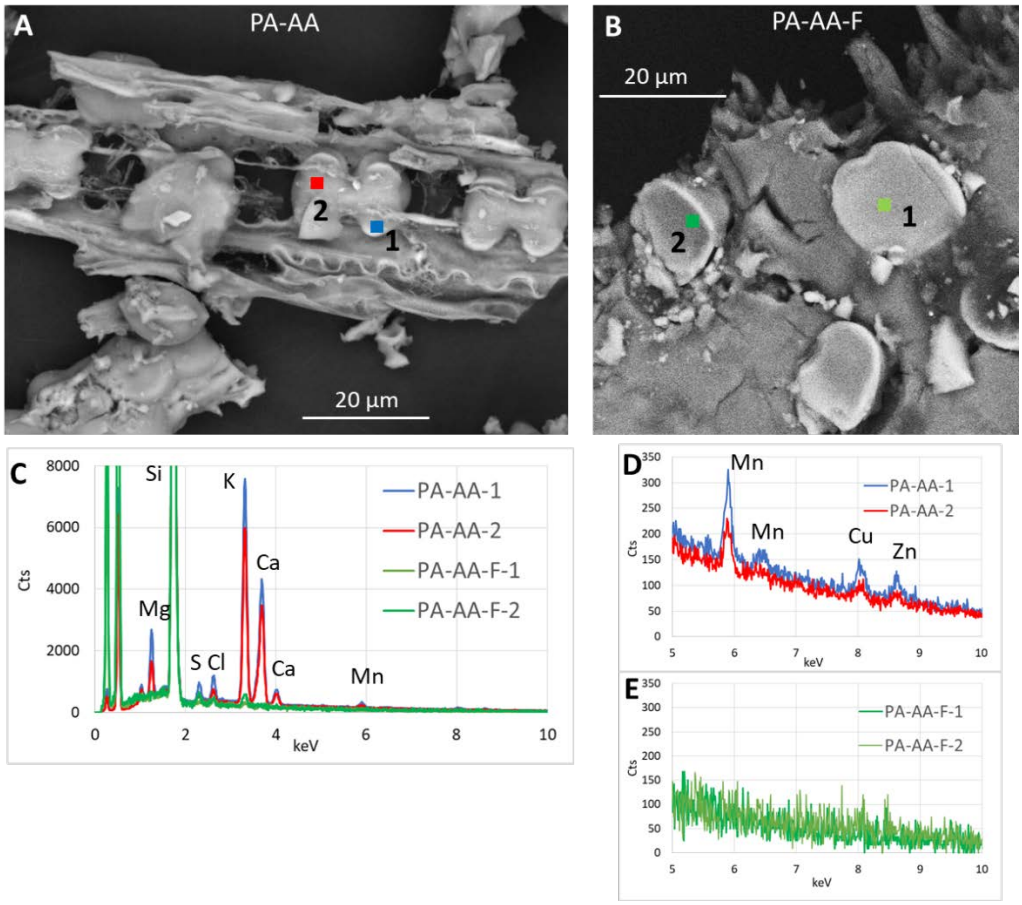

Figure 3. SEM observations of the phytoliths (A) and dry leaves (B) of *Phragmites australis* from Cartagena-La Unión (PA-AA); C: EDX spectra for the points shown in A and B; D, E: zoom on the EDX spectra in the 5-10 keV range.

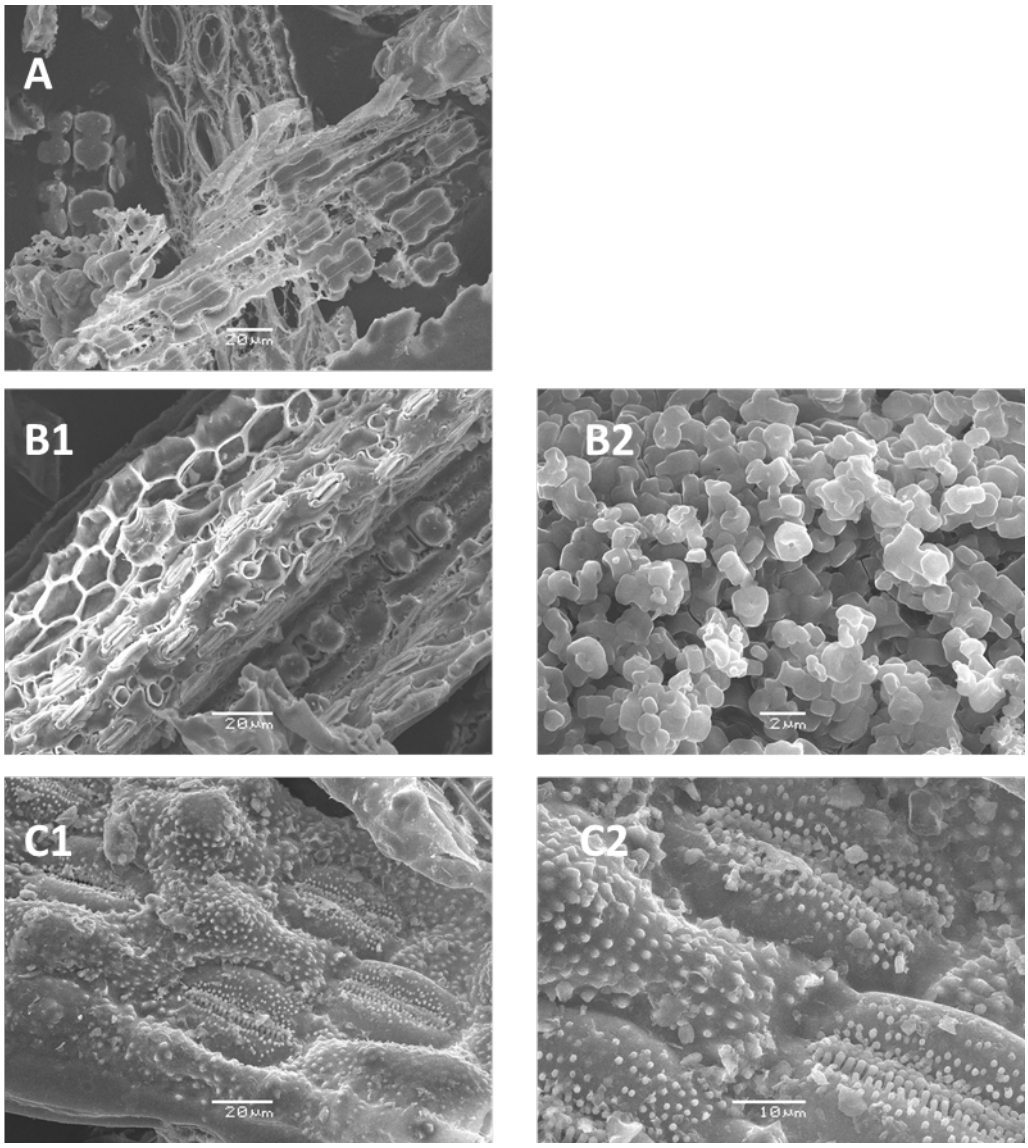

Figure 4. SEM images of purified phytoliths (A: *Arundo donax*; B1-2 : *Phragmites australis*; C1-2: *Equisetum arvense*)

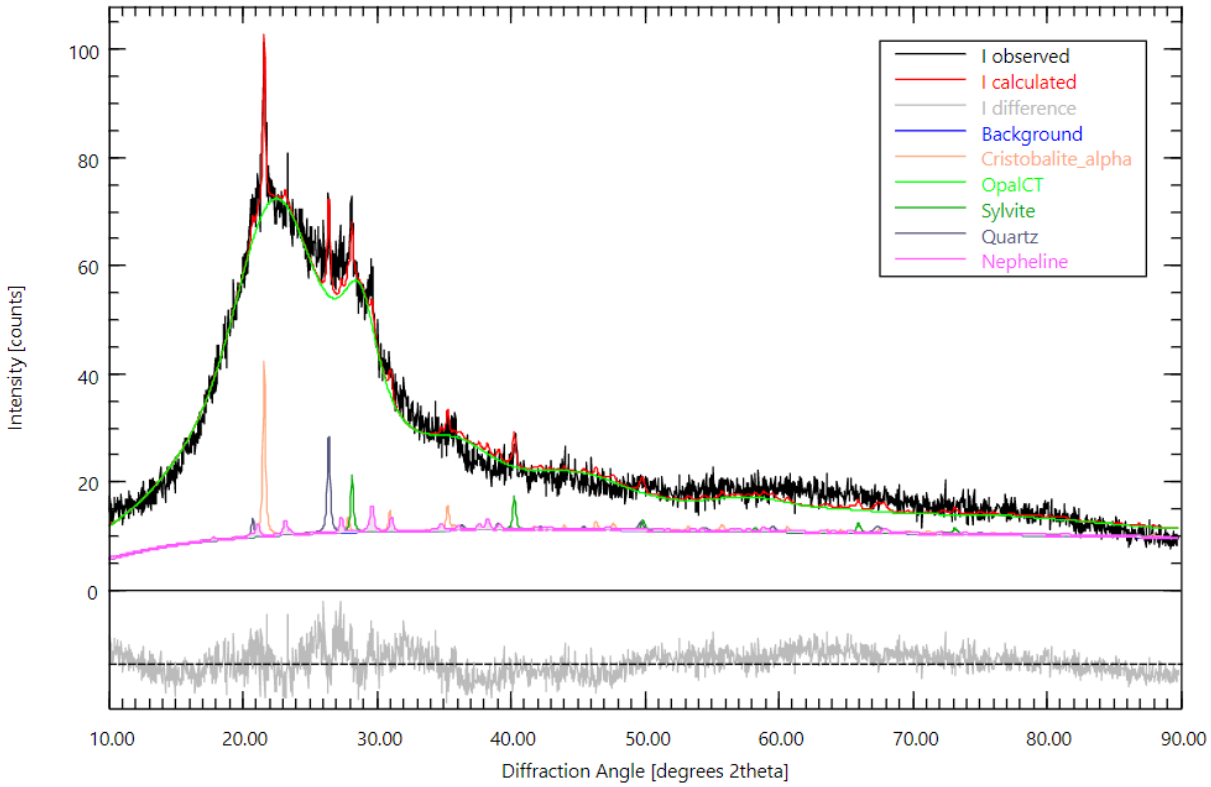

Figure 5. XRD pattern of PA-AA and Rietveld simulation. The proportion of the phases identified are listed in Table 3.

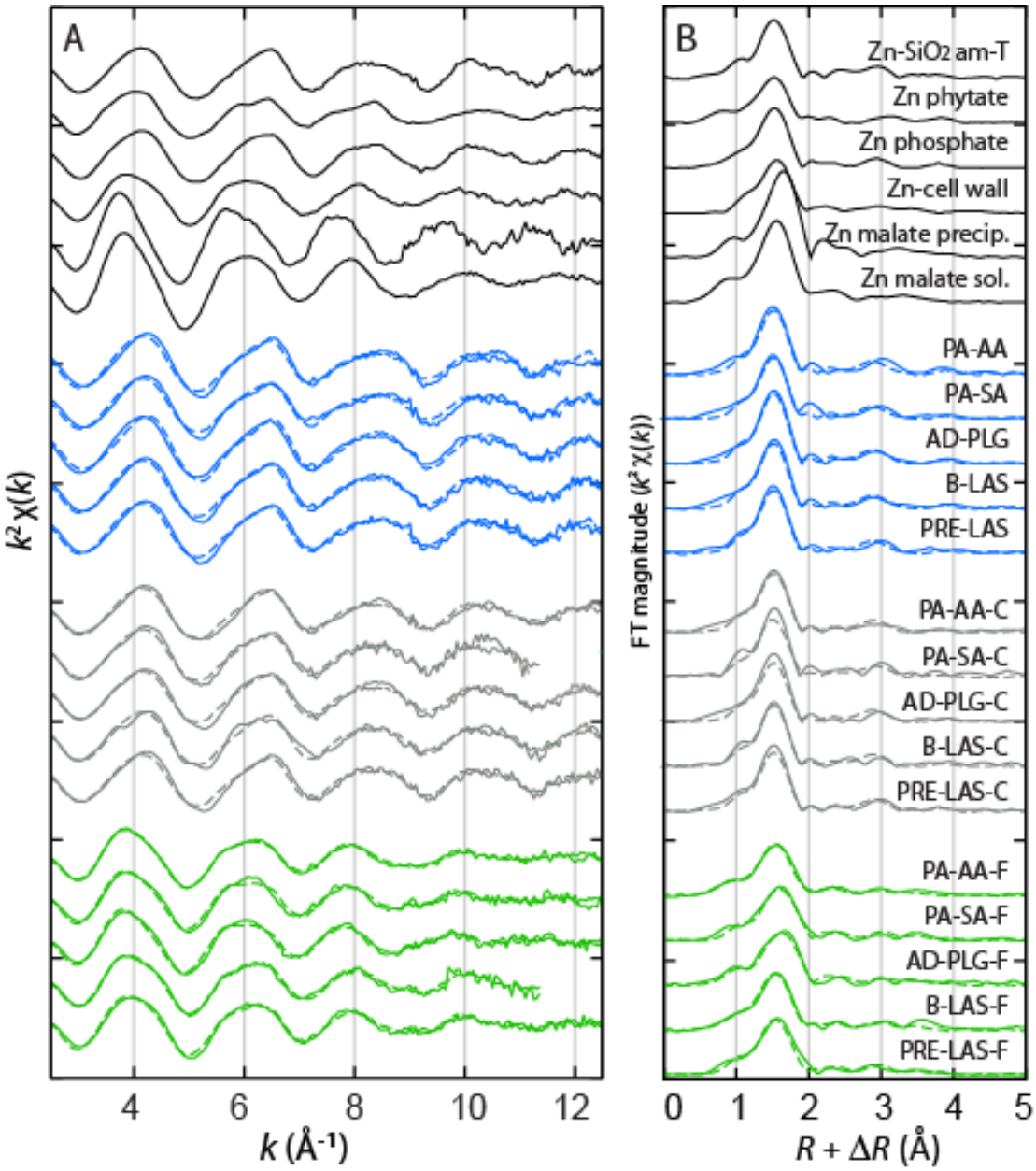

Figure 6. Zn K-edge EXAFS spectra (A) and Fourier transforms (B) for some Zn reference compounds, for the phytoliths (blue); calcinated leaves (gray) and dry leaves (green) and best linear combination fits (dashed lines).